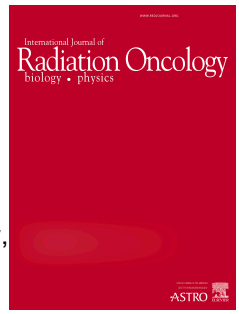

A mouse model for microbeam radiotherapy of the lung

Elisabeth Schültke, Sam Bayat, Stefan Bartzsch, Elke Bräuer-Krisch, Valentin Djonov, Stefan Fiedler, Cristian Fernandez-Palomo, Felix Jaekel, Paolo Pellicioli, Verdiana Trappetti, Guido Hildebrandt

PII: S0360-3016(20)34723-4

DOI: https://doi.org/10.1016/j.ijrobp.2020.12.030

Reference: ROB 26797

To appear in: *International Journal of Radiation Oncology • Biology • Physics*

Received Date: 24 July 2020

Revised Date: 28 October 2020

Accepted Date: 20 December 2020

Please cite this article as: Schültke E, Bayat S, Bartzsch S, Bräuer-Krisch E, Djonov V, Fiedler S, Fernandez-Palomo C, Jaekel F, Pellicioli P, Trappetti V, Hildebrandt G, A mouse model for microbeam radiotherapy of the lung, *International Journal of Radiation Oncology • Biology • Physics* (2021), doi: https://doi.org/10.1016/j.ijrobp.2020.12.030.

A mouse model for microbeam radiotherapy of the lung

Short title:

MRT model mouse lung

Elisabeth Schültke[1], Sam Bayat[2], Stefan Bartzsch[3,4], Elke Bräuer-Krisch[5], Valentin Djonov[6], Stefan Fiedler[7], Cristian Fernandez-Palomo[6], Felix Jaekel[1], Paolo Pellicioli[5], Verdiana Trappetti[6], Guido Hildebrandt[1]

[1]Department of Radiooncology, Rostock University Medical Center, Rostock, 18057, Germany
[2]STROBE Laboratory, Grenoble Alps University, Inserm UA7 and Grenoble Alps University Hospital, France
[3]Department of Radiooncology, Technical University Munich, Munich, Germany
[4]Institute for Innovative Radiotherapy, Helmholtz-Zentrum Munich (HMGU), Germany
[5]European Synchrotron Radiation Facility (ESRF), ID17 Biomedical beamline, Grenoble, France
[6]Institute of Anatomy, University of Bern, Bern, Switzerland
[7]European Molecular Laboratory (EMBL), Hamburg, Germany

Corresponding author:
Elisabeth Schültke
Department of Radiooncology, Rostock University Medical Center
Südring 75, 18059 Rostock, Germany
Tel. +49 381 494-9001
elisabeth.schueltke@med.uni-rostock.de

Funding statement
Travel and accommodation for E.S. F.J and C.F.P. to attend the experiment at the ESRF were supported by an ESRF travel grant. Dr. Schültke's work is supported by DFG grant SCHU 2589/7-1.

Conflict of interest statement:
None of the authors has any conflict of interest to disclose.

Acknowledgements
Anne Möller and Dr. Tobias Lindner (Institute of Experimental Surgery, Rostock University Medical Center) for the high-resolution CT of a reference mouse. Martin Blaschek for integrating the small animal CT data into the clinical planning system. Dr. Rika Bajorat (Department of Anaesthesia, Rostock University Medical Center) for teaching E.S. how to intubate a mouse. Dr. Stephan Kriesen (Department of Radiooncology, Rostock University Medical

Center) for building a laryngoscope small enough to intubate a mouse. Charléne Caloud and Loic St. Jean (Charles River / biomedical beamline ID 17, ESRF) for taking care of our animals at the ESRF. Alexandra Demory (biomedical beamline ID 17, ESRF) for taking care of some preparatory logistics to make our experiment at the ESRF run smoothly

Supporting material

A mouse model for microbeam radiotherapy of the lung

Detailed methods of the experimental setup

Dose calculation

A CT scan with a spatial resolution of 197 µm was obtained at the CT component of a small animal PET CT scanner (Inveon, Siemens) as basis for the dose calculation. Monte Carlo calculation was conducted for an array of quasi parallel microbeams of 50 µm width and a centre-to-centre distance of 400 µm for a field size of 3.9 × 13 mm. Since the heart is the most important organ at risk with irradiation of the thoracic cavity, the integrated dose to the heart was calculated.

Dose calculations were carried out using the Geant4 Monte Carlo tool package version 10.3.p3 and a hybrid dose calculation algorithm [1]. Monte Carlo simulations were performed sampling 10^9 photon histories from the standard MRT x-ray spectrum of the ESRF ID17 beamline according. and assuming the source published previously [2]. The dose was scored on the grid of the CT separating peak and valley dose as described in [3]. Peak dose was defined as the average dose in the central 80% of the peak region and valley dose as the average dose in the central 60% of the valley region. Hounsfield units of the planning CT were converted into material parameters following the approach of [4]. For the lung in particular homogeneous mixtures of air and water were assumed. Statistical uncertainties of the Monte Carlo simulations were below 5% in peak and valley regions. Particularly at low photon energies, dose absorption is sensitive to material composition and density. In order to minimize errors due to improper material conversion, the CT was calibrated in advance with the calibration phantom 062M (CIRS, USA). Dose deviations due to material conversions uncertainties can be reduced to around 2% by HU material calibration [5].

Unlike the brain, which has been the traditional target for MRT studies in the past, lung tissue is inhomogeneous. The typical alveolar structure with multiple non-serial interfaces between air, fluid and soft tissue make dose calculations extremely challenging. Simulations show that doses in inhomogeneous lung tissue can be vary by a factor of 1.7 [6], compared to homogeneous materials. In particular, valley doses are sensitive to dose variations due to scattering electrons travelling large distances in the air cavities.

The provided peak and valley doses were calculated assuming a homogeneous mixture of water and air, where concentrations depend on the observed Hounsfield units. Considering the fact that beam distances, electron ranges and alveolar sizes are all in the same range, this approach has to be regarded as a crude simplification. An accurate dose calculation in the lung cannot neglect the microstructure of the lung. Furthermore, the constant volume change of the organ during the respiratory cycle causes the irradiation target to move permanently under physiologic conditions. Any movement would result in the smearing of microbeam edges and thus a change in the PVDR. As a result, the normal tissue sparing effect of the microbeams would be decreased.

A more accurate simulation of microbeams in lung tissue with reasonable computational expenditure will be subject to future research.

Positioning device

In clinical radiotherapy, the accelerator head emitting the X-rays is moved around the patient in order to reach an entry point from which the X-ray beam enters the target tissue. At the synchrotron, the beam generated in the storage ring is guided through beam defining elements and vacuum pipes to the end station where its position is kept as stable as possible. In order to administer the prescribed X-ray dose, the patient, in our case a mouse, is moved through the path of the beam in vertical direction. The speed of the vertical movement through the beam and the dose rate of the incident X-ray beam determine the value of the deposited dose. A stable position during this movement is absolutely essential in order to assure precise dose deposition.

In order to simulate an anterior-to-posterior (ventral-to-dorsal) irradiation, to achieve a high dose deposition in the right lung and to limit normal tissue exposure, a specific positioning device was designed and built for this experiment. The positioning device consists of an adjustable frame mounted on motorized translation- and rotation stages which are part of the standard elements provided by the beamline. The custom-made frame allows an adjustment of its height and width in order to have a stable fixation of the animal and an unobstructed orientation of its lungs relative to the beam from different angular positions. To avoid anterior-posterior movements of the animal's body during the vertical movement of the stage, a thin PMMA plate was mounted

onto the frame to stabilize the body. A tooth hook was inserted into the upper bar of the steel frame and the animal's body was taped to the plate (Figure S1).

Animal model

The experiments were conducted at a dedicated biomedical beamline of a 3rd generation synchrotron (*exact location removed for blinded review*). All experimental protocols were approved by the Ethics Committee and by the French Ministry of Education and Research (permission number 7363-20l61 026150 13147). The animals were housed and cared for in a temperature-regulated animal facility exposed to a 12-hour light/dark cycle. All methods were carried out in accordance with relevant guidelines and regulations.

The experiments were performed on 46 healthy male C57/BL6 mice (26-30 g) obtained from Charles River France. Anaesthesia was induced by isoflurane inhalation using an induction chamber at a concentration of 2.5–3% in air, followed by intraperitoneal injection of ketamine and xylazine (ketamine:xylazine = 9:1, in a 1:10 dilution in normal saline). Once the animals were deeply anesthetized, they were placed in a supine position and immobilized.

For the intubation procedure, a cold light source was pointed at the upper thoracic cavity and neck of the animal. A custom-made retractor was used to depress the tongue, upon which the vocal cords became well visible. A 22 G canula (Introcan Safety, Braun Melsungen, catalogue number 4253540-01) where the original steel mandrin had been replaced by a plastic mandrin (Vasofix® Mandrin, Braun Melsungen, catalogue number 4215095), shortened so that it protruded from the tip of the canula only minimally, was used as a tracheal canula. It was carefully introduced between the vocal cords upon inspiration. The plastic mandrin was then removed and the correct position of the tube in the trachea was verified by briefly connecting the tube to a water lock, after which the canula was connected to a small animal respirator, providing 2.5% isoflurane in air (TEM SEGA, DeVilbiss Healthcare). The animal was positioned into the holding device (Figure 4) and volume-controlled ventilation was initiated with a tidal volume of 0.25 ml, a respiratory rate of 150, a positive end-expiratory pressure of 6 cm H_2O and FIO_2 of approximately 80 %.

Under clinical conditions in human patients, spontaneous or augmented breath hold (gating) would be the option of choice to obtain a stable treatment target. For instance, at a beam scanning speed (vertical movement of the patient through the beam) of approximately 14 mm/sec, even for a target height of seventy millimetre, a peak dose of 400 Gy could be delivered in approximately 5 seconds. Thus, the entire logistic chain including the command for breath hold, the opening of the shutter system, the irradiation and the closing of the shutter could be executed within a period of 10-12 seconds. That most patients can be expected to reliably hold their breath for the duration of such a short period of time is known from the treatment of breast cancer patients, where radiotherapy frequently is conducted under breath hold in inspiration position to reduce dose entry to the heart [7].

In animals, spontaneous breath hold is no option and augmented breath hold would require a highly refined system which could trigger irradiation always in the same position of the respiratory cycle. Thus, eliminating physiologic lung movement by induction of apnoea is the most easily feasible method to assure that the target region is in the same position during the entire duration of the irradiation procedure. Considering that the administration of several hundred Gy in the peak dose takes less than half a minute, irradiation is feasible under oxygen insufflation without lasting damage to the animal. By setting a constant positive end expiratory pressure (PEEP) during irradiation, we were able to standardize the experiment throughout all experimental groups, which is important for an accurate morphological reproduction of the irradiation geometry in the tissue.

After the end of the irradiation process, the isoflurane supply was shut off, the animal was removed from the holding device and placed in prone position on a second small animal respirator until spontaneous breathing resumed. The animal was then extubated and placed for recovery in a warm cage. Once moving around again on its own, the animal was placed back into its normal cage.

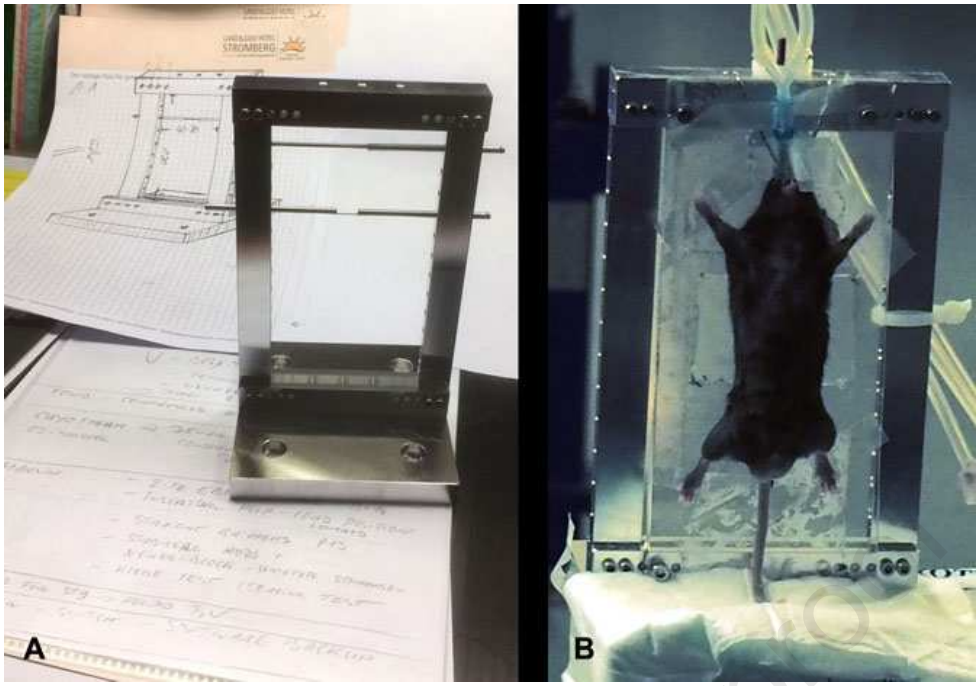

Figure S1. Original design of the frame (A) and the animal positioned in the holding device (B).

Pre-irradiation imaging

Pre-irradiation imaging in irradiation position was conducted to assure that the heart was outside the irradiation field.

At the biomedical beamline ID17, pink-beam imaging with a fast alignment procedure was developed [8]. In this normal tissue study of mouse lung, the target to be irradiated was visualized by projection images and the irradiation field was defined by the individual anatomical landmarks of each mouse. For every animal, one image was obtained and the irradiation field was adjusted accordingly by a lateral and /or horizontal translation of the animal in order to avoid the heart, respecting a safety margin of ~1 mm.

The wiggler gap was opened to 100 mm in order to reduce the extremely high photon flux and as a result the applied dose. A 2D X-ray detector setup was installed about 3 meters downstream the animal goniometer support. The detector is a Fast Readout Low Noise camera (FReLoN based on a 2048x2048 CCD chip coupled with a scintillator and an optical lenses system [9]. The ultimate pixel size is 23 µm but the resolution can be adjusted by binning to obtain a good compromise between a sub-millimetric resolution (approx. 100 µm) and a reasonable contrast at a dose as low as possible in a field of view of up to 50 mm in height.

Irradiation procedure

In irradiation mode, the wiggler was set to its minimum gap (24.8 mm) in order to benefit from the maximum available photon flux. Attenuators were adjusted to obtain the spectrum that is standardly used for MRT at this beamline, typically 50-350 keV with a maximum intensity at 102keV [10]. The beam defining slits were adjusted to the planned irradiation field. The multislit collimator was inserted in the beam and the FReLoN camera was removed into a radiation protecting lead cabinet. Those changes in the experimental setup between imaging and irradiation modes are carried out automatically, which allows to toggle between the two modes within a very short time (less than 4 min). Sub-millimetric targeting is made possible by using the same beam for imaging and irradiation, without the need for repositioning of the animal between the two procedures.

Targeting the right lung of the animals, we irradiated with an array of quasi-parallel microbeams of 50 µm width and a centre-to-centre distance of 400 µm. The field size was 3.9 mm (width) × 13 mm (height), corresponding

to 9 microbeams. Peak entrance doses were 40 Gy or 400 Gy and the valley doses were approx. 0.42 and 4.2 Gy, respectively. Thus, the peak-to-valley dose ratio calculated using Monte Carlo was approximately 95 at a depth of 3 mm. The dose rate under broad beam reference conditions was measured according to the protocol described by Fournier et al. [11] for a 2 cm × 2 cm field in 2 cm depth. Monte Carlo calculated peak and valley dose profiles were calibrated with respect to these reference conditions.

At machine storage ring currents between 154.7 mA and 196.9 mA, dose rates between 69.3 Gy/sec/mA and 70.5 Gy/sec/mA were achieved. Thus, even peak doses of 400 Gy were easily deposited within a few seconds. However, the spontaneous respiration rate of 80 or more per minute in adult mice breaks down to more than one respiration cycle per second. The lung volume difference between inspiration and expiration positions in a mouse is significant at approximately 50 % of the functional residual capacity [12]. With an overall irradiation time of approximately 10 s, the lung excursions throughout the respiratory cycles would prevent a dose deposition in a microbeam pattern with clearly defined peak and valley dose zones. Exact dose calculation would be extremely difficult in this case, if at all possible. More importantly, as a consequence of the respiratory lung excursions, the valley dose zones which determine the normal tissue tolerance would receive much higher X-ray doses. This would result in a higher degree of normal tissue damage. In order to assure that the prescribed peak doses are deposited in the tissue according to the planned irradiation pattern, a stable body position was secured and the controlled ventilation was paused at a PEEP of 10 cm H_2O during irradiation.

Of the 46 mice, 36 underwent microbeam irradiation of the right lung. Eighteen mice each were irradiated with a peak dose of 40 Gy and 400 Gy, respectively. Depending on the electron storage ring current, the animals were moved through the beam along the z-axis with a speed of between 14.58 mm/sec and 17.52 mm/ s to deliver a peak entrance dose of 400 Gy. In order to deliver a peak entrance dose of 40 Gy, the horizontal slits defining the beam height were changed from 500 micron to 100 micron and the speed of the movement along the z-axis was varied between 26 and 35 mm/ sec depending again on the electron storage ring current.

Radiosensitive Gafchromic™ film was used to record the irradiation pattern. It showed that there was a runout problem of the motorized stage, which was used to move the animals vertically through the beam. This caused some lateral displacement of the microbeam array at the time of our experiment, however, the microbeams were still parallel even after the displacement. That the vibration was due to the runout of the mechanical system and not due to respiration of the animal was verified by moving a film without an animal through the beam on the same motorized stage. The patterns recorded with and without the animals on the stage were identical.

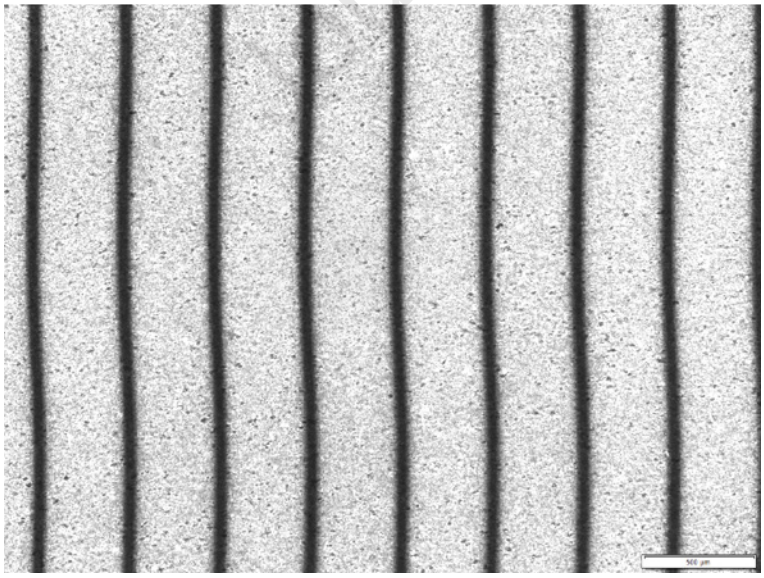

Figure S2. Irradiation pattern recorded on Gafchromic™ film.

Tissue harvesting and immunofluorescent staining

Animals were sacrificed and lungs were harvested at 24, 48 and 72 hours after irradiation (n=6/group). Four animals underwent apnoea and ventilation but no irradiation. Six healthy male mice served as non-irradiated and non-ventilated controls.

The harvesting method for the lung tissue is crucial to preserve tissue morphology in correlation to the irradiation pattern. The procedure used in this experiment is described as follows:

Mice were sacrificed with an intraperitoneal injection of sodium pentobarbital (200mg/kg BW). An incision was made in the skin of the anterior part of the neck and the trachea was exposed. Thus, a *post-mortem* tracheotomy was performed, a 20 G catheter (32 mm length) was placed into the trachea for circa 1/3 of its length and fixed with a 4-0 surgical thread. The abdomen was opened and an incision was made in the diaphragm to open the thoracic cavity. Mice were perfused though the right ventricle of the heart with 5 ml 1x PBS to flush out the blood that exited from an incision made in the vena cava inferior. Then, the tracheotomy catheter was connected to a 10 ml syringe containing the fixative solution (2% PFA in 1x PBS buffered at pH 7.4). The syringe must be positioned at the exact height of 20 cm from the surface of the work bench in order to provide the optimal pressure to fix the lung in the inspiration position. Once the PFA solution stopped flowing and the lungs were completely filled with the fixative, the tracheotomy catheter was removed and the trachea was tied with a suture. Finally, the lungs were gently dissected from the rib cage. After an overnight fixation in PFA, the lungs were incubated in a solution of 40% sucrose in distilled water for 24 hours. Next, the lungs were embedded in a 7.5% gelatine and 15% solution (Sigma, catalogue number 1040700500) and stored at -80°. Cryostat sections of 50 µm thickness were mounted for immunofluorescent staining. The sections were incubated with rabbit anti-gamma H2AX-phospho S139 (Abcam ab11174) as primary antibody followed by the donkey anti-rabbit secondary Ab Alexa Fluor488 (Life technologies A-21206) and DAPI. Images were acquired with a Zeiss LSM 880 confocal microscope. Eight serial z-slices were acquired for a total z image size of 24 µm. Images are shown as maximum intensity projection.

The graph in Figure S2 illustrates the increasing gamma H2AX staining intensity between 24 hours and 72 hours after irradiation. To obtain these values, the five most intense areas of the gamma H2AX stain in high resolution images were chosen and the median green value (in arbitrary intensity units) was determined in a 50 µm x 50 µm field using the colour histogram function of Image J [13]. All images were obtained with identical image acquisition parameters.

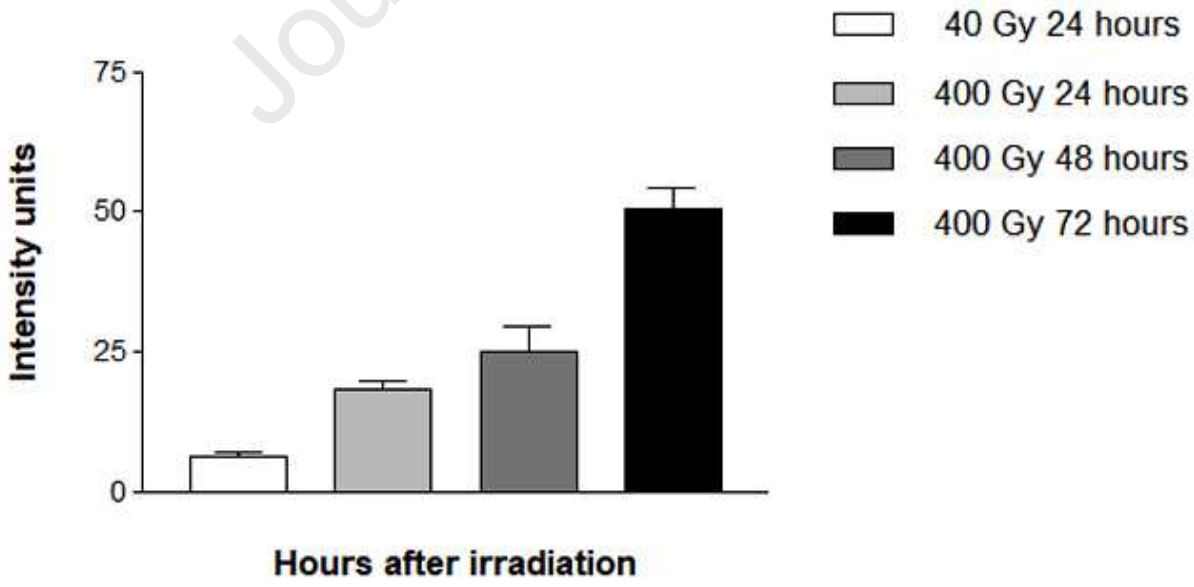

Figure S3. The gamma H2AX staining intensity increased continuously within the first 72 hours after irradiation.

The median values are 6.3 (3.9-8.4) for 40 Gy at 24 hours, 18.4 (15.2-21.9) for 400 Gy at 24 hours, 24.9 (16.6-37.2) for 400 Gy at 48 hours and 50.5 (38.4-59.9) for 400 Gy at72 hrs after irradiation.

References

1. Donzelli, M., Bräuer-Krisch,, E., Oelfke U. Wilkens J.J. & Bartzsch S. Hybrid dose calculation: a dose calculation algorithm for microbeam radiation therapy. Phys. Med. Biol. 63(4), 045013 (2018).
2. Bartzsch, S., Lerch, M., Petasecca, M., Bräuer-Krisch,, E. & Oelfke U. Influence of polarization and a source model for dose calculation in MRT. Med. Phys. 41(4), 041703 (2014).
3 Debus, C., Oelfke, U. . Bartzsch, S. A point kernel algorithm for microbeam radiation therapy. Phys. Med. Biol. 62(21), 8341 (2017).
4. Schneider, W., Bortfeld, T. & Schlegel, W. Correlation between CT numbers and tissue parameters needed for Monte Carlo simulations of clinical dose distributions. Phys. Med. Biol. 45(2), 459 (2000).
5. Rong, Y., Smilowitz, j., Tewatia, D., Tomé, W.A. & Paliwal, B. Dose calculation on kV cone beam CT images: an investigation of the Hu-density conversion stability and dose accuracy using the site-specific calibration. Med. Dos. 35(3), 195-207 (2010).
6. Hombrink, G., Wilkens, J.J., Combs, S.E., Bartzsch, S. Simulation and measurement of microbeam dose distribution in lung tissue. Physica Medica. 75, 77-82, doi: 10.1016/j.ejmp.2020.06.003 (2020).
7. Nguyen, M.H., Lavilla M., Kim, J.N. & Fang, L.C. Cardiac sparing characteristics of internal mammary chain radiotherapy using deep inspiration breath hold for left-sided breast cancer. Radiat. Oncol. 13(1), 103, doi:10.1186/s13014-018-1052-8 (2018).
8. Nemoz, C., Kibleur, A., Hyacinthe, J.N., Berruyer, G., Brochard, T., Bräuer-Krisch, E., Le Duc, G., Brun, E., Elleaume, H. & Serduc, R. In vivo pink-beam imaging and fast alignment procedure for rat brain tumor radiation therapy. J. Synch. Radiat. 23(1), 339-43, doi:10.1107/S1600577515018561 (2016).
9. Coan, P., Peterzol, A, Fiedler, S., Ponchut, C., Labiche, J.C. & Bravin, A.. Evaluation of imaging performance of a taper optics CCD; FReLoN' camera designed for medical imaging. J. Synch. Radiat. 13(Pt 3), 260-70 (2006).
10. Crosbie, J.C., Fournier, P., Bartzsch, S., Donzelli, M., Cornelius, I., Stevenson, A.W., Requardt, H. & Bräuer-Krisch, E. Energy spectra considerations for synchrotron radiotherapy trials on the ID17 bio-medical beamline at the European Synchrotron Radiation Facility. J. Synch. Radiat. 22(4), 1035-41, doi:10.1107/S1600577515008115 (2015).
11. Fournier, P., Crosbie, J.C., Cornelius, I., Berkvens, P., Donzelli, M., Clavel, A.H., Rosenfeld, A.B., Petasecca, M., Lerch, M.L. & Bräuer-Krisch, E. Absorbed dose-to-water protocol applied to synchrotron-generated x-rays at very high dose rates. Phys. Med. Biol. 61(14), N349-61, doi: 10.1088/0031-9155/61/14/N349 (2016).
12. Lundblad, L.K., Thompson-Figueroa, J., Leclair, T., Irvin, C.G. & Bates, J.H. Thoracic gas volume measurements in paralyzed mice. An. iomed. Eng. 32, 1420-1427 (2004).
13. Schindelin, J., Arganda-Carreras, I., Frise, E., Kaynig, V., Longair, M., Pietzsch, T., Preibisch, S., Rueden, C., Saalfeld, S., Schmid, B., Tinevez, J.Y., White, D.J., Hartenstein, V., Eliceiri, K., Tomancak, P. & Cardona, A. Fiji: an open-source platform for biological-image analysis. Nat. Meth. 9, 676-682 (2012).

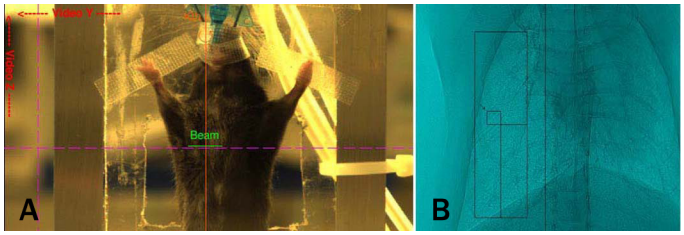

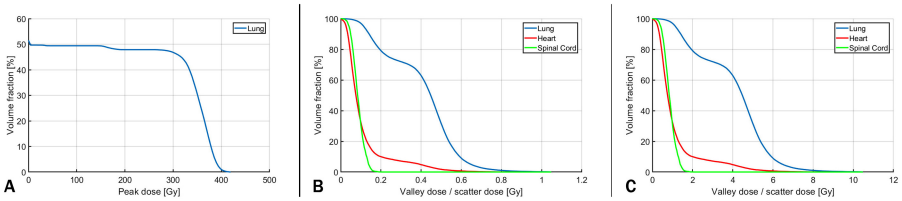

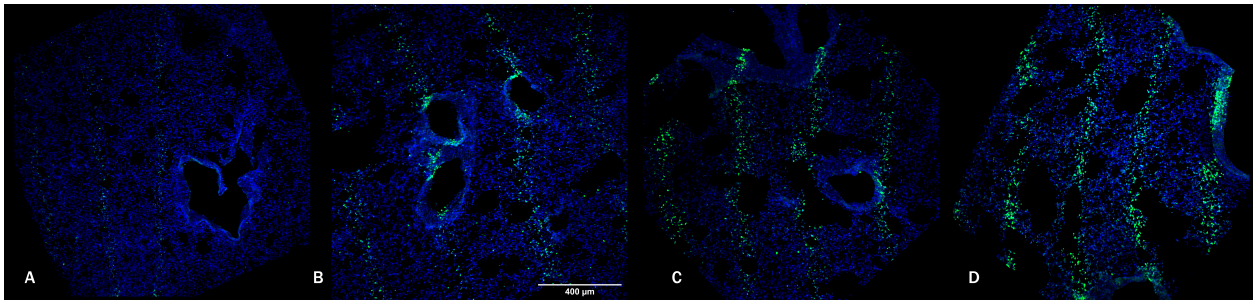

A mouse model for microbeam radiotherapy of the lung

ABSTRACT

Purpose: Radiotherapy is an important treatment component for patients with lung cancer. However, the survival time gained with clinical radiotherapy techniques is relatively short.

Data from pre-clinical experiments suggest that synchrotron microbeam radiotherapy (MRT) could be much better suited to control malignant brain tumours than current clinical concepts of radiotherapy. Even at peak doses of several hundred Gy, the extent of functional deficits is amazingly low.

Methods and Materials: We have developed the first mouse model to study the effects of microbeam irradiation in lung tissue.

Results: Up to peak doses of 400 Gy, no acute adverse effects were seen.

Conclusion: This model is well suited to explore the potential of MRT in the treatment of lung cancer, the response of normal lung tissue and organs of risk.

Introduction

Lung cancer is reported with an incidence between 33.9 and 60 in 100,000, accounting for more than 10% of all new cancer cases annually. [1,2]. For many of those patients, radiotherapy is an essential component of the interdisciplinary therapeutic approach.

Dose prescription to the lung is limited because of a high risk to develop pneumonitis, an inflammatory condition of the lung tissue caused by irradiation which frequently results in lung fibrosis, leading to a severely reduced quality of life [3]. The fairly recent concept of stereotactic body radiotherapy (SBRT) offers patients with small lung tumours a much shorter treatment concept. However, such concepts are applicable only to a limited number of small peripheral lesions. High toxicity has been observed after treatment for central lesions.

Stereotactic radiotherapy works on the basis of spatial dose fractionation at the milimeter range. Over the last decades, the new concept of microbeam radiotherapy (MRT) has been developed in pre-clinical studies. MRT can be considered stereotactic radiosurgery with spatial dose fractionation at the micrometer range. In brain tissue, it has already been shown in small animal models of malignant brain tumours that the tumour control and normal tissue sparing achieved with MRT are superior, compared to broad beam irradiation [4,5,6]. The better morphologic preservation of normal tissue structures resulted in a well-sustained brain function in small and large animal models [7,8].

Two phantom studies of microbeam irradiation in the lung were published in the 1990s [9,10].

We have now designed and conducted the first feasibility study to investigate the acute response of lung tissue to microbeam irradiation in mice.

Materials ad Methods

The experiments were conducted at a dedicated biomedical beamline of a 3rd generation synchrotron. All experimental protocols were approved by the Ethics Committee and by the French Ministry of Education and Research (permission number 7363-20l61 026150 13147).

A fixed space multislit collimator, the design of which has been described in detail previously [11], was inserted into the X-ray beam generated by the synchrotron source to generate an array of quasi parallel microbeams. The result was an inhomogeneous dose distribution with periodically alternating sequences of peak dose (high dose) zones and valley dose (low dose) zones in the target tissue. The individual beam width was 50 µm and the centre-to-centre distance was 400 µm.

Before irradiating the animals, absolute dosimetry was performed following the protocol developed by Fournier et al. [12]. The active volume of a PTW PinPoint ionization chamber (Type 31014, PTW, Freiburg, Germany) was aligned in the center of a 20 × 20 mm² field and placed at 20 mm depth in a water-equivalent plastic cube phantom to determine the beam dose rate. The ionization chamber was calibrated at TH200 radiation source to match the energy spectrum of the synchrotron radiation used in this experiment. The minimum field size measurable by the PinPoint chamber was respected. Under these reference conditions, the dose rate of the X-ray beam was determined in Gy/s/mA with an uncertainty of 4.4% (2σ). At the

beginning of each irradiation procedure, the actual electron current of the synchrotron storage ring was considered in order to determine the dose rate in Gy/s to deliver the prescribed target dose.

Healthy male C57/BL6 mice obtained from Charles River France underwent microbeam irradiation of the right lung with an array of quasi-parallel microbeams. General anaesthesia with isoflurane, tracheal intubation and mechanical ventilation allowed a reliable induction of an inspiratory apnoea of a duration of approximately 10 seconds, that was sufficiently long to conduct microbeam irradiation at peak doses up to 400 Gy. The duration of the entire procedure, including the induction of anaesthesia and intubation, positioning of the animal in the beam and irradiation, ranged between 15 and 20 minutes.

Since no previous studies existed regarding the response of cardiac tissue and the impulse conduction system of the heart to the high MRT peak doses, irradiation of the heart was avoided. Pre-irradiation imaging was conducted in irradiation position and the position of the animal was corrected where necessary to assure that the heart was outside the irradiation field (Figure 1).

The typical alveolar structure of the lung with its multiple non-serial interfaces between air, fluid and soft tissue makes dose calculation extremely challenging [13]. The peak and valley doses were calculated assuming a homogeneous mixture of water and air, where concentrations depended on the observed Hounsfield units of CT scan obtained with a spatial resolution of 197 µm using the CT component of a small animal PET CT scanner (Inveon, Siemens). This CT scan was also used to outline the heart and the spinal cord as organs of risk. Monte Carlo calculation

with the Geant4 tool package was conducted for a field size of 3.9 × 13 mm, corresponding to 9 vertical microbeams, in the right lung of the animals. Uncertainties of the Monte Carlo simulations for peak and valley doses are estimated below 7%.

A more detailed description of the experimental setup is provided as supporting material.

Results

We conducted a pilot experiment with two different peak doses (n=18/group). The peak entrance doses were 40 Gy and 400 Gy and the valley doses were nominally 0.42 Gy and 4.2 Gy, respectively. Thus, the peak-to-valley dose ratio at the beam entrance was approximately 95 at a depth of 3 mm. The dose on the heart, the most important organ of risk with irradiation of the thoracic cavity, was calculated to be on average 0.11 Gy for a peak dose of 40 Gy and 1.1 Gy for a peak dose of 400 Gy (Figure 2).

No signs of potential adverse effects due to pulmonal or cardiac toxicity such as audible breath sounds, pulmonary distress or decrease of general activity were seen in the mice at any time during the 72 hours observation period after microbeam irradiation. No motor deficits as signs of spinal cord toxicity were observed. The observation was conducted continuously for approx. one hour after the irradiation in a wake-up room setting, in two-hourly intervals for the following eight hours and three times daily thereafter.

Aiming for a constant post-end-expiratory pressure (PEEP) during irradiation, we were able to standardize the experiment throughout all experimental groups. Furthermore, we also

successfully standardized the harvest of the lung tissue, to reproduce the irradiation morphology as close as possible. The gamma H2AX immunostain, representing the number of DNA double strand breaks caused by the irradiation, resulted in intense fluorescence along the microbeam paths in all irradiated groups. After irradiation with peak doses of 400 Gy, the intensity of the immunofluorescence was increasing continuously during the first three days after irradiation (Figure 3 and Supplementary Figure S3). This can be explained by delayed cell death due to secondary processes, including radiation-induced bystander effects. The intensity of the gamma H2AX stain along the microbeam paths is significantly lower after irradiation with peak doses of only 40 Gy.

Discussion

This was the first time that the lung of mice was chosen as target organ for microbeam irradiation. We have shown that no acute adverse effects occurred after MRT with peak doses up to 400 Gy.

In the current study, the irradiation dose was based on Monte Carlo simulations designed to simulate both the reference conditions and the irradiation geometry in the animals. An experimental dosimetry study for the microbeam irradiation was not performed. The development of specific phantoms to reproduce the irradiation geometry in the animals in combination with high resolution detectors could be an interesting theme for future studies.

The diameter of an alveolus, the structural unit in which the gas exchange takes place, is about 200 μm in humans and 35-45 μm in mice [14]. Thus, dose calculation in human patients might

be somewhat easier with respect to the changes of air / fluid / soft tissue interfaces, but more demanding because of the increase in scatter expected in the larger target areas in human patients, which would result in a decrease of the PVDR [10].

To allow irradiation of irregular (not rectangular) shaped targets without risking functional cardiac damage, the experimental setup should be refined. One could introduce a multileaf collimator which allows the temporary blocking of microbeam paths in analogy to clinical radiotherapy. Another solution might be the insertion of a radiopaque mask protecting the heart. Provided that a low toxicity profile can be shown also in long-term studies after MRT in the lung, we suggest to test a scenario where MRT is used as a simultaneously integrated boost (SIB) in a clinical radiotherapy schedule, in order to achieve a higher single fraction dose. Clinically, the SIB concept has been shown to result in longer local recurrence-free survival in patients with NSCLC [15]. This could be an especially interesting approach in patients with a low percentage of PD-L1 positive tumour cells reported in the initial histology.

A high percentage of PD-L1 positive cells within a tumour correlates to a high responsiveness of the tumour to newly developed check-point inhibitors and thus to a better tumour control and longer survival times [16]. Recent data suggest that hypofractionated radiotherapy might support the induction of PD-L1. This radiotherapy-induced PD-L1 expression has been reported to be stable and long-lasting *in vitro* as well as clinically [17,18,19]. MRT can be considered a hypofractionated radiotherapy approach par excellence, with between one and three fractions reported in the literature. It would be interesting to follow up the work hypothesis that MRT

induces the check point inhibitor PD-L1 and thus improves tumour responsiveness to immunotherapy.

With its extremely good preservation of normal tissue function observed previously in brain tissue, MRT might also prove to be a good approach to increase both the quality of life and the recurrence free interval for patients with lung cancer.

Conclusion

Microbeam irradiation studies in the lung of mice are technically feasible, although technically challenging. The mouse model can therefore be considered a suitable tool for further preclinical studies focused on the treatment of lung cancer and the study of normal tissue tolerance.

References

1. World Cancer Research Fund International: www.wcrf.org

2. Death cause statistics 2013, Federal Agency for Statistics, Wiesbaden, Germany, 2014.

3. Schröder, C., Engenhart-Cabillic, R., Vorwerk, H., Schmidt, M., Huhnt, W., Blank, E., Sidow, D. & Buchali, A. Patient's quality of life after high-dose radiation therapy for thoracic carcinomas : Changes over time and influence on clinical outcome. Strahlenther. Onkol. PMID: 27787567 (2016).

4. Potez, M., Bouchet. A., Flaender, M., Rome, C., Collomb, N., Grotzer, M., Krisch, M., Djonov, V., Balosso, J., Brun, E., Laissue, J.A. & Serduc, R. Synchrotron X-Ray boost delivered by microbeam radiation therapy after conventional X-Ray therapy fractionated in time improves

F98 glioma control. Int. J. Radiat. Oncol. Biol. Phys. 07(2), 360-369, doi:10.1016/j.ijrobp.2020.02.023 (2020).

5. Bouchet, A., Potez, M., Coquery, N., Rome, C., Lemasson, B., Bräuer-Krisch, E., Rémy, C., Laissue, J., Barbier, E.L., Djonov, V. & Serduc, R. Permeability of brain tumor vessels induced by uniform or spatially microfractionated synchrotron radiation therapies. Int. J. Radiat. Oncol. Biol. Phys. 98(5), 1174-1182, doi:10.1016/j.ijrobp.2017.03.025 (2017).

6. Bouchet, A., Bräuer-Krisch E., Prezado, Y., El Atifi, M., Rogalev, L., Le Clec'h, C., Laissue, J.A., Pelletier, L. & Le Duc, G. Better Efficacy of Synchrotron spatially microfractionated radiation therapy than uniform radiation therapy on glioma. Int. J. Radiat. Oncol. Biol. Phys. 95(5), 1485-1494, doi:10.1016/j.ijrobp.2016.03.040 (2016).

7. Schültke, E., Juurlink, B.H., Ataelmannan, K., Laissue, J., Blattmann, H., Bräuer-Krisch, E., Bravin, A., Minczewska, J., Crosbie, J., Taherian, H., Frangou, E., Wysokinsky, T., Chapman, L.D., Griebel, R. & Fourney, D. Memory and survival after microbeam radiation therapy. Eur. J. Radiol. 68(3 Suppl), S142-6, doi:10.1016/j.ejrad.2008.04.051 (2008).

8. Laissue, A., Blattmann, H., Wagner, H.P., Grotzer, M.A. & Slatkin, D.N. Prospects for microbeam radiation therapy of brain tumours in children to reduce neurological sequelae. Dev. Med. Child. Neurol. 49(8), 577-81 (2007).

9. Company, F.Z. & Allen, B.J. Calculation of microplanar beam dose profiles in a tissue/lung/tissue phantom. Phys. Med. Biol. 43, 2491–2501 (1998).

10. Company, F.Z. Calculation of dose profiles in stereotactic synchrotron microplanar beam radiotherapy in a tissue-lung phantom. Australas. Phys. Eng. Sci. Med. 30(1), 33-41 (2007).

11. Bräuer-Krisch, E., Requardt, H., Brochard, T., Berruyer, G., Renier, M., Laissue, A. & Bravin, A. New technology enables high precision multislit collimator for microbeam radiation therapy. Rev.Sci.Instrum. 80(7), doi: 10.1063/1.3170035 (2009).

12. P. Fournier, Crosbie, J.C., Cornelius, I., Berkvens, P., Donzelli, M., Clavel, A.H., Rosenfeld, A.B., Petasecca, M., Lerch, M.L. & Bräuer-Krisch, E. Absorbed dose-to-water protocol applied to synchrotron-generated x-rays at very high dose rates, Phys. Med. Biol. 161(14), N349-61, N349-61, doi: 10.1088/0031-9155/61/14/N349 (2016).

13. Hombrink, G., Wilkens, J.J., Combs, S.E., Bartzsch, S. Simulation and measurement of microbeam dose distribution in lung tissue. Physica Medica. 75, 77-82, doi: 10.1016/j.ejmp.2020.06.003 (2020).

14. Soutiere, S.E., Tankersley, C.G. & Mitzner, W. Differences in alveolar size in inbred mouse strains. Respir. Physiol. Neurobiol. 140(3), 283-91 (2004).

15. Qiu, B., Li, Q.W., Ai, X.L., Wang, B., Huan, J., Zhu, Z.F., Yu, G.H., Ji, M., Jiang, H.H., Li, C., Zhang, J., Chen, L., Guo, J.Y., Zhou. Y. & Liu, H. Investigating the loco-regional control of simultaneous integrated boost intensity-modulated radiotherapy with different radiation fraction sizes for locally advanced non-small-cell lung cancer: clinical outcomes and the application of an extended LQ/TCP model. Radiat. Oncol. 15(1), 124, doi:10.1186/s13014-020-01555-x (2020).

16. Guirgis, .HM. The impact of PD-L1 on survival and value of the immune check point inhibitors in non-small-celllung cancer; proposal, policies and perspective. J. Immunother. Cancer. 6(1), 15, doi:10.1186/s40425-018-0320-3 (2018).

17. Narits, J., Tamm, H & Jaal, J. PD-L1 Induction in tumor tissue after hypofractionated thoracic radiotherapy for non-small cell lung cancer. Clin. Transl. Radiat. Oncol. 22, 83-87, doi:10.1016/j.ctro.2020.04.003 (2020).

18. Gong, X., Li, X., Jiang, T., Xie, H., Zhu, Z., Zhou, F. & Zhou, C. Combined radiotherapy and anti-PD-L1 antibody synergistically enhances antitumor effect in non-small cell lung cancer. J. Thorac. Oncol. 12(7), 1085-1097, doi:10.1016/j.jtho.2017.04.014 (2027).

19. Shen, M.J., Xu, L.J., Yang, L., Tsai, Y., Keng, P.C., Chen, Y., Lee, S.O. & Chen, Y. Radiation alters PD-L1/NKG2D ligand levels in lung cancer cells and leads to immune escape from NK cell cytotoxicity via IL-6-MEK/Erk signaling pathway. Oncotarget. 8(46), 80506-80520, doi:10.18632/oncotarget.19193 (2017).

Figure legends

FIGURE 1.

Screen shot of the control room terminal with the animal positioned in the beam (A) and the pre-irradiation X-ray image (B), both with the beam array entry zone marked.

FIGURE 2.

Dose-volume histogram (DVH) for peak dose and valley doses expected for the non-irradiated lung, the heart and the spinal cord after microbeam irradiation with peak doses of 40 Gy (B) and 400 Gy (C). Similar to the valley dose curves, the shape of the curves for peak doses of 40 Gy and 400 Gy is identical but the values differ by a factor of 10.

FIGURE 3.

Microphotographs of lung tissue after gamma H2AX immunostain.

The staining intensity is much less intense at 24 hours after irradiation with peak doses of 40 Gy (A), as compared to 400 Gy (B). The staining intensity increases continuously until the end of the observation period at 72 hours after irradiation, as shown in the immunofluorescence images at 48 hours (C) and 72 hours (D) after irradiation with peak doses of 400 Gy.